PROCEEDINGS OF SCIENCE

Current status of the neutral pion multiplicity studies at CLAS12

Marshall B. C. Scott[a,*] **for the CLAS12 collaboration**

[a] *Argonne National Laboratory,*
9700 S Cass Ave, Lemont, United States of America

E-mail: scottmar@umich.edu

Multiplicity studies are a fundamental measurement of particle physics, detailing the production fraction of a particle species within a more general particle process. Studies of hadron multiplicities within Semi-Inclusive Deep Inelastic Scattering (SIDIS) use the non-perturbative generation of hadrons from lepton-nucleon scattering to delve into the nature of the hadronization process. Being that this process is the convolution of the perturbative electromagnetic hard scattering cross section, and the non-perturbative quark parton distributions and fragmentation functions, multiplicity studies can help reveal information about the non-perturbative structure of the proton. Moreover, the transverse momentum of the final state hadrons provides insight into the transverse momentum and spin of the fragmenting partons. This work involves the SIDIS production of neutral pions at CLAS12, the CEBAF Large Acceptance Spectrometer for 12 GeV, where a 10.6 GeV electron beam was scattered off a fixed liquid hydrogen target in the fall of 2018. We present the current status of the neutral pion multiplicity studies at CLAS12.

25th International Spin Physics Symposium (SPIN 2023)
24-29 September 2023
Durham, NC, USA

*Speaker

PoS(SPIN2023)068

1. Introduction

Semi-Inclusive Deep Inelastic Scattering (SIDIS) seeks to resolve the internal structure of a hadron and gain insight into the subsequent fragmentation process by using leptons interacting electromagnetically with the partons within the hadron and detecting the products generated from these interactions. This work investigates the hadronization of neutral pions by way of extracting multiplicities using SIDIS of electrons scattering off of a liquid hydrogen target. Neutral pions or π^0s are described in the Parton model as a superposition of the first generation of quark-antiquark pairs, $(u\bar{u}-d\bar{d})/\sqrt{2}$, posses a mass of 0.134977 GeV, and predominately decay into two photons [1].

The one photon exchange SIDIS hadronic production cross section of an unpolarized electron and an unpolarized target is described as

$$\frac{d\sigma^h}{dx_B dQ^2 dz dP_{hT}^2 d\phi_h} = \frac{\pi\alpha_e^2}{xQ^4}\frac{y^2}{(1-\varepsilon)}\left(1+\frac{\gamma^2}{2x}\right)\times \left\{F_{UU,T}+\varepsilon F_{UU,L}+\sqrt{2\varepsilon(1+\varepsilon)}\cos(\phi_h)F_{UU}^{\cos(\phi_h)}+\varepsilon\cos(2\phi_h)F_{UU}^{\cos(2\phi_h)}\right\}, \quad (1)$$

with the first two subscripts of the structure functions, $F_{UU,T/L}$, denoting that the electron and proton are unpolarized, and the T(L) subscripts detailing the transverse (longitudinal) polarization of the exchanged photon [2]. The kinematic regime is spanned by $x_B = Q^2/2P\cdot q$, $Q^2 = -q^2$, $z = P\cdot P_h/P\cdot q$, ϕ_h, the angle between the hadron momentum and the lepton scattering plane in the center of mass frame, and P_{hT}^2, the square of the transverse component of the hadron's momentum perpendicular to the lepton scattering plane. P is the momentum of the target, P_h is the momentum of the hadron, and q is the difference between the initial (l) and final (l') lepton momentum. On the right side of the equation is the fine structure constant, α_e, the elasticity, $y = P\cdot q/P\cdot l$,

$$\varepsilon = \frac{1-y-\frac{1}{4}\gamma^2y^2}{1-y+\frac{1}{2}y^2+\frac{1}{4}\gamma^2y^2}, \quad (2)$$

and $\gamma = 2Mx/Q^2$, with M being the mass of the target. Removing $F_{UU,T}+\varepsilon F_{UU,L}$ from the bracket and arranging terms in Eq. 1, we arrive at

$$\frac{d\sigma^h}{dx_B dQ^2 dz dP_{hT}^2 d\phi_h} = A\left(1+B\cos(\phi_h)+C\cos(2\phi_h)\right). \quad (3)$$

Within the Parton model, the $F_{UU,T}$ structure function can be described as a collinear parton distribution function (PDF) coupled with an ansatz Gaussian transverse momentum distribution, i.e.,

$$F_{UU,T} = \sum_q e_q^2 x_B \int d^2\mathbf{k}_\perp \frac{f_q(x_B)\, e^{-k_\perp^2/\langle k_\perp^2\rangle}}{\pi\langle k_\perp^2\rangle}\frac{D_q(z)\, e^{-P_{h\perp}^2/\langle P_{h\perp}^2\rangle}}{\pi\langle P_{h\perp}^2\rangle}, \quad (4)$$

with the sum including all quarks and antiquarks (q), and the integral is over the transverse quark momenta ($\mathbf{k}_\perp$) [3]. e_q is the charge of the quark or antiquark, f_q is the PDF of quark or antiquark q, describing the number density of quark or antiquark within the target, and $D_q(z)$ is the fragmentation function (FF) describing the probability of said quark or antiquark generating hadron h. The perpendicular momentum terms, $k_\perp$ and $P_{h\perp}$, are the lightcone transverse momenta of the

parton and the final hadron with respect to the parton, respectively. The transverse momentum widths within the Gaussian terms, $\langle P_{h\perp}^2 \rangle$ and $\langle k_\perp^2 \rangle$, are model dependent and can depend on x_B and z, respectively. Integrating and using the relation $\langle P_{hT}^2 \rangle = z^2 \langle k_\perp^2 \rangle + \langle P_{h\perp}^2 \rangle$ [4], $F_{UU,T}$ can be rewritten as

$$F_{UU,T} = \sum_q e_q^2 x_B \frac{f_q(x_B)\, D_q(z)\, e^{-P_{hT}^2/\langle P_{hT}^2 \rangle}}{\pi \langle P_{hT}^2 \rangle}. \tag{5}$$

Neutral pion production is related to the $D_q(z)$ FF with the primary generating quarks being the valence quarks, two up quarks and one down quark within the proton, and up and down and their antiquark partners within the sea.

The hadronic multiplicity, M_h, is defined the ratio of the hadronic production cross section to the deep inelastic scattering (DIS) cross section. The leading order (LO) DIS cross section is defined as

$$\frac{d\sigma^{DIS}}{dx_B dQ^2} = \frac{2\pi\alpha_e^2}{x_B Q^4} \frac{y^2}{(1-\varepsilon)} \left(1 + \frac{\gamma^2}{2x_B}\right) \sum_q e_q^2 x_B f_q(x_B), \tag{6}$$

and the full multiplicity is then

$$\begin{aligned} M_h &\equiv \frac{d\sigma^h}{dx_B dQ^2 dz dP_{hT}^2 d\phi_h} \Bigg/ \frac{d\sigma^{DIS}}{dx_B dQ^2} \\ &= \frac{1}{2\sum_q e_q^2 f_q(x_B)} \times \sum_q e_q^2 f_q(x_B) D_q(z) \frac{e^{-P_{hT}^2/\langle P_{hT}^2 \rangle}}{\pi \langle P_{hT}^2 \rangle} \left(1 + B\cos(\phi_h) + C\cos(2\phi_h)\right), \end{aligned} \tag{7}$$

where we have neglected the $\varepsilon F_{UU,L}$ term, which is typically small compared to the $F_{UU,T}$ term in the limit of small M^2/Q^2 and P_{hT}^2/Q^2 [4].

2. The CLAS12 Detector

This study uses data taken during the fall of 2018 data taking period in Hall B at Jefferson Laboratory using the CEBAF Large Acceptance Spectrometer at 12 GeV (CLAS12) detector. The CLAS12 detector is divided into 6 sectors providing a full azimuthal coverage and houses two main detector systems: the Forward Detector (FD) and the Central Detector (CD). The center of the FD is located about 7 meters from the target, possesses a polar angle coverage between 5 and 40 degrees, and houses a torus, drift chambers, a low threshold Chrenkov counter, and a forward time of flight detector. The CD is located approximately 0.5 meters from the target and contains a solenoid, silicon vertex tracker, and a central time of flight detector. A schematic of the CLAS12 detector is shown in Fig. 1 with a full discussion of the detector can be found in Ref. [5].

There have been previous SIDIS multiplicity measurements at COMPASS and HERMES. COMPASS published charged pion multiplicities at low x_B using muon scattering off of ^{6}LiD [6], and HERMES published charged and neutral pion multiplicities using positron on liquid hydrogen scattering with an average $x_B < 0.1$ [7], and charged pion data from electron and positron scattering on liquid hydrogen and deuterium targets [8]. CLAS12 seeks to extend the SIDIS multiplicity kinematic range to higher x_B as shown in Fig. 2 below.

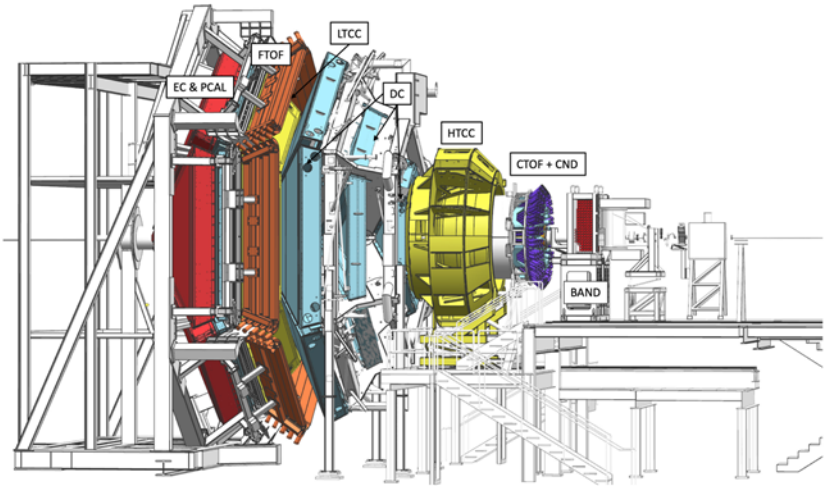

Figure 1: Depiction of the CLAS12 spectrometer [9].

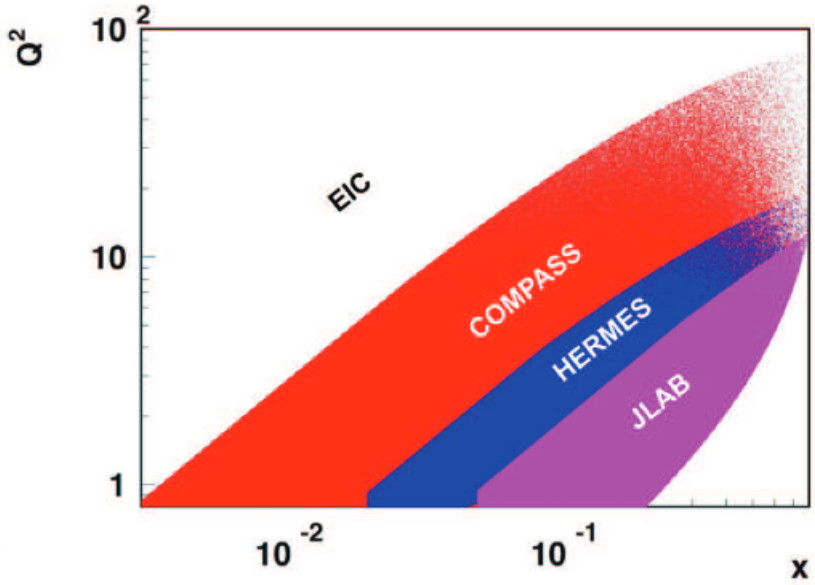

Figure 2: Comparison of the $x_B - Q^2$ kinematic coverages between COMPASS, HERMES, the EIC, and CLAS12 [10].

3. Data Analysis

The data used in this work utilized a 10.6 GeV polarized electron beam scattering off of a liquid hydrogen target with zero net electron polarization. Event selection was based upon detecting a single scattered electron and at least two photons in the FD. The monte carlo used was a SIDIS generator based upon PEPSI, a polarized electron generator, and LEPTO [11]. The data was subject to general quality cuts and fiducial cuts were implemented on the monte carlo to improve data-monte carlo agreement. In addition, kinematic cuts were made to the data and monte carlo, yielding good agreement between many of the kinematic variables. A comparison between the data and monte

carlo of a sample of these variables, the six kinematic variables related to the differential cross section, i.e., x_B, Q^2, z, p_T^2, ϕ_h, and $m_{\gamma\gamma}$ (the invariant mass of the two photons from the neutral pion decay) is shown in Fig. 3. For these plots, each variable of interest has been integrated over all other variables, and the data and monte carlo parent distributions have been normalized so that the number of events are the same.

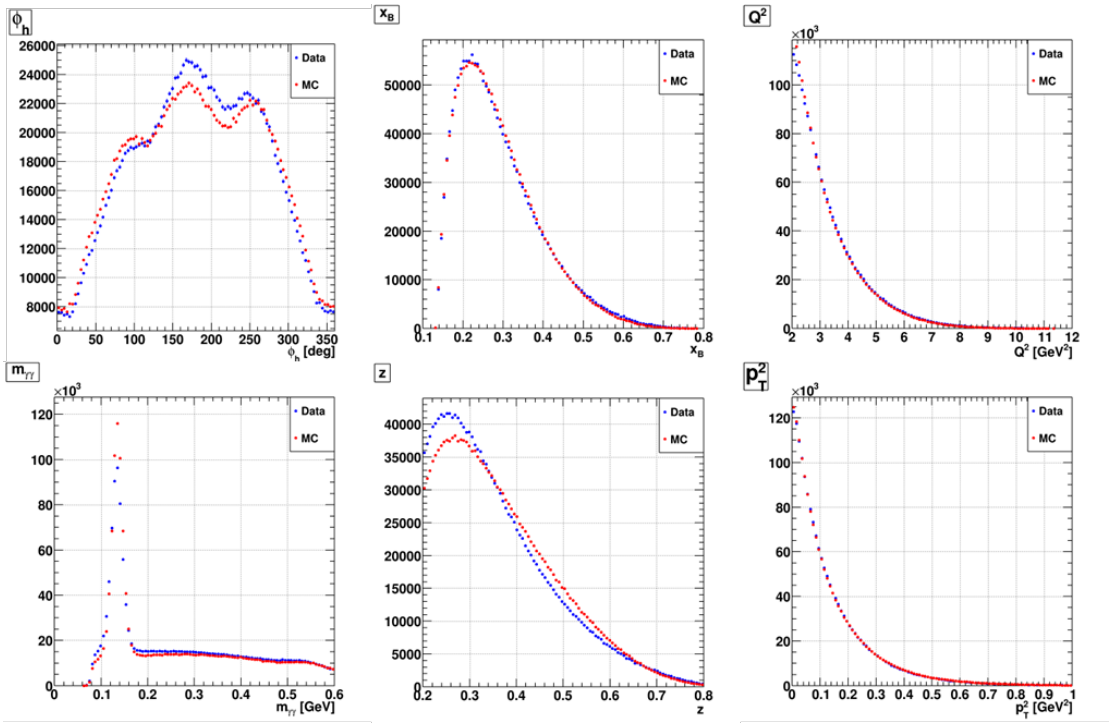

Figure 3: Comparison of the data and monte carlo kinematic variables, with data depicted in blue and monte carlo depicted in red. In the top row ϕ_h, x_B, and Q^2 are plotted from left to right, and in the bottom row $m_{\gamma\gamma}$, z, and p_T^2 are plotted from left to right.

For this preliminary work, ϕ_h was integrated over, so Eq. 7 reduces to

$$\begin{aligned} M_h &\equiv \frac{d\sigma^h}{dx_B dQ^2 dz dP_{hT}^2} \Big/ \frac{d\sigma^{DIS}}{dx_B dQ^2} \\ &= \frac{1}{\sum_q e_q^2 f_q(x_B)} \times \sum_q e_q^2 f_q(x_B) D_q(z) \frac{e^{-P_{hT}^2/\langle P_{hT}^2\rangle}}{\langle P_{hT}^2\rangle}. \end{aligned} \tag{8}$$

The kinematic phase space was divided into 8 $x_B - Q^2$ bins and 64 $z - p_T^2$ bins within each of those $x_B - Q^2$ bins, as depicted in Fig. 4.

Within each of the $x_B - Q^2 - z - p_T^2$ bins, the $\gamma\gamma$ invariant mass distribution is generated from all possible photon pairs within an event and fit with a combination of a Gaussian for the neutral pion mass peak region and a four-dimensional polynomial describing the background. The number of neutral pions was then extracted from the fit.

The measured neutral pion multiplicity is defined as

$$M_h(x_B, Q^2, z, p_T^2) = \frac{dN_{\pi^0}}{dx_B dQ^2 dz dP_{hT}^2} \Big/ \left(\frac{dN_{DIS}}{dx_B dQ^2} \times A(x_B, Q^2, z, p_T^2) \right), \tag{9}$$

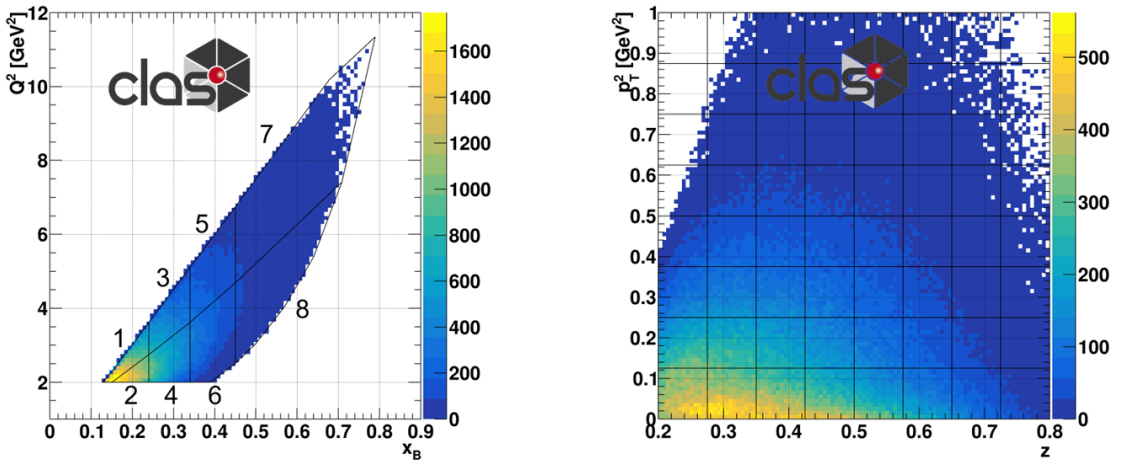

(a) $x_B - Q^2$. **(b)** $z - p_T^2$.

Figure 4: An illustration of the neutral pion multiplicity kinematic phase space with the 8 $x_B - Q^2$ bins shown on the left and the 64 $z - p_T^2$ bins show on the right.

with

$$\frac{dN_{\pi^0}}{dx_B dQ^2 dz dP_{hT}^2} \tag{10}$$

being the number of neutral pions measured within the four-dimensional kinematic bin,

$$\frac{dN_{DIS}}{dx_B dQ^2} \tag{11}$$

is the number of DIS electrons within the two-dimensional $x_B - Q^2$ bin, and $A(x_B, Q^2, z, p_T^2)$ is the four-dimensional acceptance. For this preliminary analysis, we assume that the electron efficiency of the SIDIS channel is the same as the efficiency in the DIS channel. Consequently, the extracted bin-by-bin acceptance, strictly speaking the product of the acceptance and efficiency, is the ratio of the reconstructed neutral pion distribution to the generated neutral pion distribution, holding that the generated pion distribution stems from an event with a well reconstructed electron.

4. Results

The multiplicities as a function of z in the 8 p_T^2 bins for each of the 8 $x_B - Q^2$ bins is illustrated in Fig. 5. The results show a clear trend of decreasing multiplicities as z and p_T^2 increase. Moreover, as p_T^2 increases, there is a decrease in statistics and acceptance at the edges of the z distributions, which led to those bins being removed from the results.

To compare with theoretical predictions, multiplicities as functions of z were calculated by integrating over the p_T^2 bins. These p_T^2 integrated multiplicities are shown in Fig. 6, accompanied by LO theoretical curves with a 1 σ error band. The LO theoretical multiplicity is found by integrating Eq. 8 with respect to p_T^2, which yields

$$M_h = \frac{\sum_q e_q^2 f_q(x_B) D_q(z)}{\sum_q e_q^2 f_q(x_B)}. \tag{12}$$

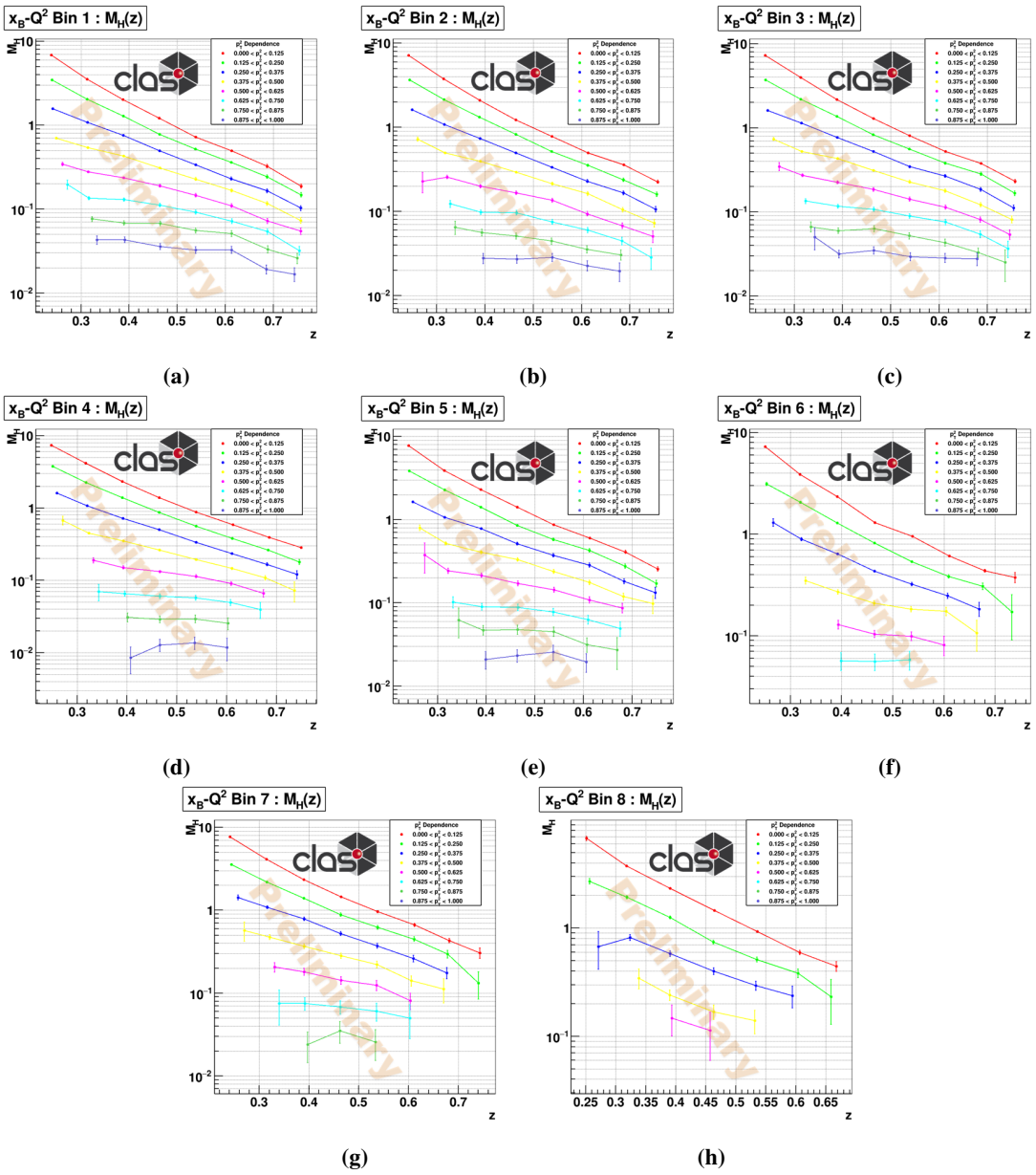

Figure 5: Extracted neutral pion multiplicities with statistical errors as functions of z in each of the 8 p_T^2 bins for each of the 8 $x_B - Q^2$ kinematic bins : $x_B - Q^2$ bin 1 (a), $x_B - Q^2$ bin 2 (b), $x_B - Q^2$ bin 3 (c), $x_B - Q^2$ bin 4 (d), $x_B - Q^2$ bin 5 (e), $x_B - Q^2$ bin 6 (f), $x_B - Q^2$ bin 7 (g), and $x_B - Q^2$ bin 8 (h).

The theoretical extraction of the multiplicity involved all quark and antiquark flavors except the top, and utilized the CT10nlo PDF sets [12]. Two different FF sets were studied, the NNFF1.1h [13] and the MAPFF1.0 [14]. When using the FF sets, the mean of the sum of the charged pion FFs was used due to the quark-antiquark content of the charged pion sum being equal to that of the neutral pion, i.e., $(u\bar{d} + d\bar{u})$ for the charged pions and $(u\bar{u} - d\bar{d})$ for the neutral pion [7].

There is a marketed difference between the NNFF and the MAPFF results, with the NNFF results yielding systematically higher multiplicity curves than the MAPFF. This could stem from

the NNFF only using single inclusive hadron production from electron-positron annihilation data, while MAPFF also includes charged multiplicity data from HERMES [7] and COMPASS [6]. When restricted to single inclusive hadron production data, the NNFF and the MAPFF are much closer in agreement [14].

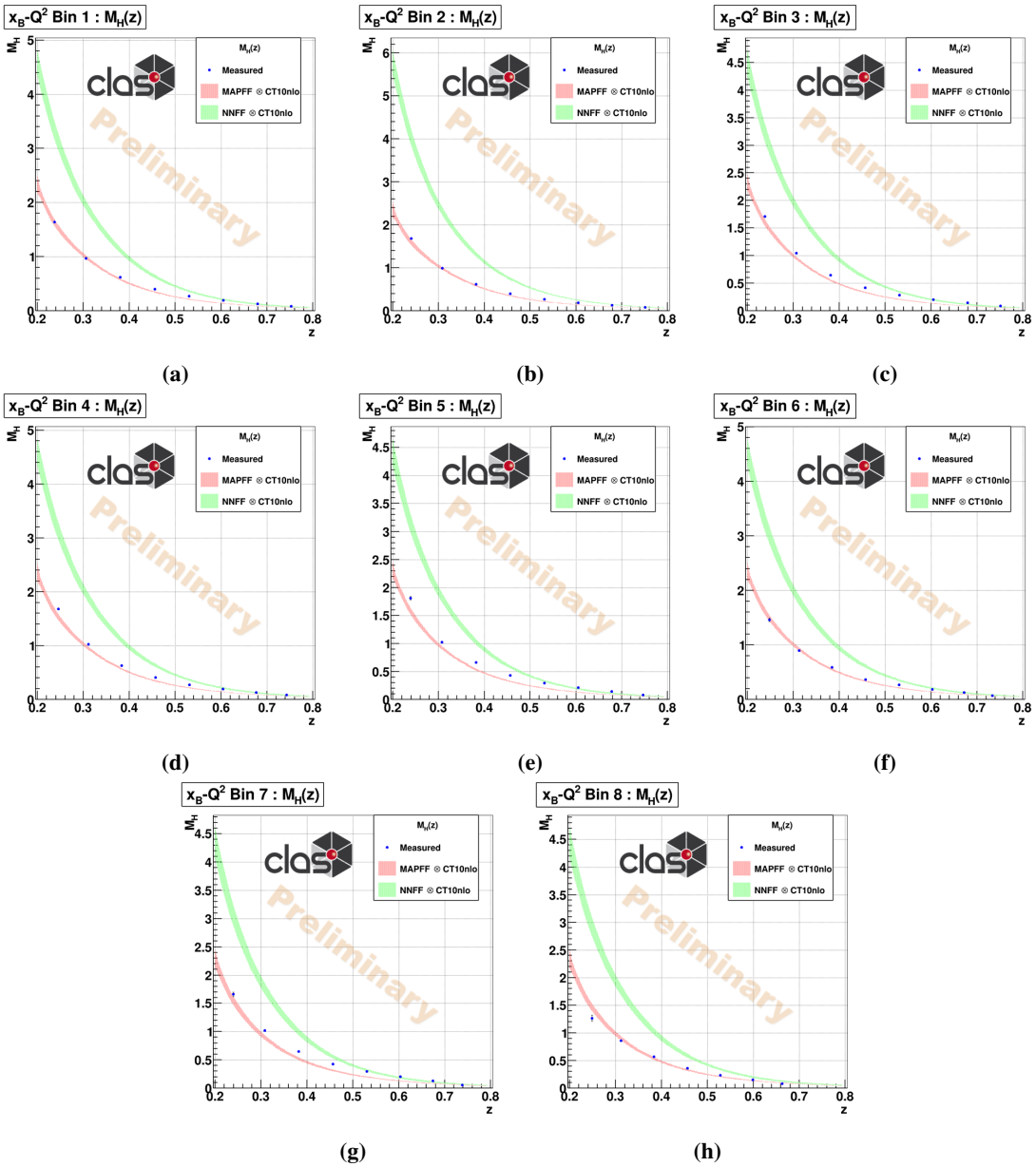

Figure 6: p_T^2 integrated neutral pion multiplicity with as functions of z in $x_B - Q^2$ bins 1 (a), 2 (b), 3 (c), 4 (d), 5 (e), 6 (f), 7 (g), and 8 (h). The LO theory curves using the CT10nlo PDFs, and the NNFF and MAPFF functions are depicted in green and red, respectively. The multiplicities are plotted with statistical errors, and the LO theory curves are depicted with a 1 σ error band.

5. Conclusion and Outlook

Utilizing SIDIS electron on proton scattering data and the CLAS12 detector, the preliminary neutral pion multiplicities were extracted in the $x_B - Q^2 - z - p_T^2$ four-dimensional kinematic phase space. The multiplicities show a general trend of decreasing as z and p_T^2 increase. By integrating over p_T^2, the preliminary multiplicities as a function z were extracted and shown to be inline with the LO theory predictions utilizing the MAPFF fragmentation functions and the CT10nlo PDFs. Current work has been focused on rebinning the kinematic phase space, fitting the invariant mass distribution within each ϕ_h bin and extracting the A term from Eq. 3 as the number neutral pions, and incorporating unfolding methods for acceptance corrections. To conclude this analysis, studies on the electron efficiency and radiative corrections must be performed.

References

[1] R. L. Workman *et al.* [Particle Data Group], PTEP **2022**, 083C01 (2022) doi:10.1093/ptep/ptac097

[2] A. Bacchetta, M. Diehl, K. Goeke, A. Metz, P. J. Mulders and M. Schlegel, JHEP **02**, 093 (2007) doi:10.1088/1126-6708/2007/02/093 [arXiv:hep-ph/0611265 [hep-ph]].

[3] X. Yan *et al.* [Jefferson Lab Hall A], Phys. Rev. C **95**, no.3, 035209 (2017) doi:10.1103/PhysRevC.95.035209 [arXiv:1610.02350 [nucl-ex]].

[4] A. Signori, A. Bacchetta, M. Radici and G. Schnell, JHEP **11**, 194 (2013) doi:10.1007/JHEP11(2013)194 [arXiv:1309.3507 [hep-ph]].

[5] V. D. Burkert, L. Elouadrhiri, K. P. Adhikari, S. Adhikari, M. J. Amaryan, D. Anderson, G. Angelini, M. Antonioli, H. Atac and S. Aune, *et al.* Nucl. Instrum. Meth. A **959**, 163419 (2020) doi:10.1016/j.nima.2020.163419

[6] C. Adolph *et al.* [COMPASS], Eur. Phys. J. C **73**, no.8, 2531 (2013) [erratum: Eur. Phys. J. C **75**, no.2, 94 (2015)] doi:10.1140/epjc/s10052-013-2531-6 [arXiv:1305.7317 [hep-ex]].

[7] A. Airapetian *et al.* [HERMES], Eur. Phys. J. C **21**, 599-606 (2001) doi:10.1007/s100520100765 [arXiv:hep-ex/0104004 [hep-ex]].

[8] A. Airapetian *et al.* [HERMES], Phys. Rev. D **87**, 074029 (2013) doi:10.1103/PhysRevD.87.074029 [arXiv:1212.5407 [hep-ex]].

[9] V. Burkert *et al.* [CLAS], Eur. Phys. J. A **57**, no.6, 186 (2021) doi:10.1140/epja/s10050-021-00474-z [arXiv:2103.12651 [nucl-ex]].

[10] H. Avakian, A. Bressan and M. Contalbrigo, Eur. Phys. J. A **52**, no.6, 150 (2016) [erratum: Eur. Phys. J. A **52**, no.6, 165 (2016)] doi:10.1140/epja/i2016-16150-x

[11] G. Ingelman, A. Edin and J. Rathsman, Comput. Phys. Commun. **101**, 108-134 (1997) doi:10.1016/S0010-4655(96)00157-9 [arXiv:hep-ph/9605286 [hep-ph]].

[12] J. Gao, M. Guzzi, J. Huston, H. L. Lai, Z. Li, P. Nadolsky, J. Pumplin, D. Stump and C. P. Yuan, Phys. Rev. D **89**, no.3, 033009 (2014) doi:10.1103/PhysRevD.89.033009 [arXiv:1302.6246 [hep-ph]].

[13] V. Bertone *et al.* [NNPDF], Eur. Phys. J. C **77**, no.8, 516 (2017) doi:10.1140/epjc/s10052-017-5088-y [arXiv:1706.07049 [hep-ph]].

[14] R. A. Khalek *et al.* [MAP (Multi-dimensional Analyses of Partonic distributions)], Phys. Rev. D **104**, no.3, 034007 (2021) doi:10.1103/PhysRevD.104.034007 [arXiv:2105.08725 [hep-ph]].